Received: 1 June 2018 | Revised: 18 September 2018 | Accepted: 21 September 2018

DOI: 10.1002/mrm.27566

NOTE

Magnetic Resonance in Medicine

Whole brain measurements of the positive BOLD response variability during a finger tapping task at 7 T show regional differences in its profiles

Yohan Boillat[1] | **Wietske van der Zwaag**[2,3]

[1]Laboratory for Functional and Metabolic Imaging, Ecole Polytechnique Fédérale de Lausanne, Lausanne, Switzerland

[2]Biomedical Imaging Research Center, Ecole Polytechnique Fédérale de Lausanne, Lausanne, Switzerland

[3]Spinoza Centre for Neuroimaging, Amsterdam, Netherlands

Correspondence
Yohan Boillat, Laboratory for Functional and Metabolic Imaging, LIFMET-CIBM, Station 6, École Polytechnique Fédérale de Lausanne, CH-1015 Lausanne, Switzerland.
Email: yohan.boillat@epfl.ch
Twitter: @YohanBoillat

Funding information
Centre d'Imagerie BioMédicale of the Universités de Lausanne, Université de Genéve, Hôpitaux Universitaires Genéve, Centre Hospitalier Universitaire Vaudois, and Ecole Polytechnique Fédérale de Lausanne; the Leenaards and Jeantet Foundations; and the Swiss National Science Foundation (31003A_149983 and 31003A_153070)

Purpose: The positive BOLD response can vary across brain regions. Here, the positive BOLD responses of motor regions, including the cerebellum, were investigated by fast fMRI acquisition.

Methods: The participants were asked to perform an event-related finger-tapping task in a 7T MRI scanner during a fast 3D-EPI controlled aliasing in parallel imaging acquisition protocol (CAIPI; TR = 399 ms). The positive BOLD responses of 6 motor regions were extracted and their timings and shapes measured.

Results: Compared with other brain regions, the positive BOLD responses in the cerebellum and secondary somatosensory cortex showed delayed onsets, but no differences were observed for the time to-peak. Additionally, variations of the undershoot and main peak amplitudes were also observed, and undershoot was quasi-absent in the cerebellum.

Conclusion: This study confirms that care should be taken when drawing conclusions about neuronal activity from the BOLD signal, particularly for the cerebellum.

KEYWORDS
BOLD response, cerebellum, fast acquisition, fMRI, hemodynamic response function, motor cortices

1 | INTRODUCTION

Task-driven BOLD-fMRI studies use the link between neuronal activity and blood dynamics to study brain activation. The BOLD response[1,2] is caused by local changes in the concentration of deoxygenated hemoglobin. The T_2^*-weighted MRI acquisitions are sensitive to the BOLD signal, and fast acquisition methods such as EPI are ideal for observing the transient signal changes associated with neuronal activation.

Following a short stimulus, the positive BOLD response (PBR) shows a very characteristic shape. The PBR rises shortly after stimulus onset, peaking 6-8 seconds later, followed by a decrease that goes below the baseline level—the so-called poststimulus undershoot—and finally a return to baseline (Figure 1A). The occurrence of an initial dip before the positive BOLD signal increase has been described[3,4] and is less well established.

Previous studies have observed that the PBR varies in terms of shape and timing among subjects[5,6] and brain regions,[5] and is influenced by substance consumption (e.g., caffeine[7]), stimulus conditions,[8] age,[9] and brain pathologies.[10] These variations could be driven by neuronal activity,[11] metabolic demands,[12] or vascular compliance.[13] Therefore, a simple motor task may yield different PBRs in different people,

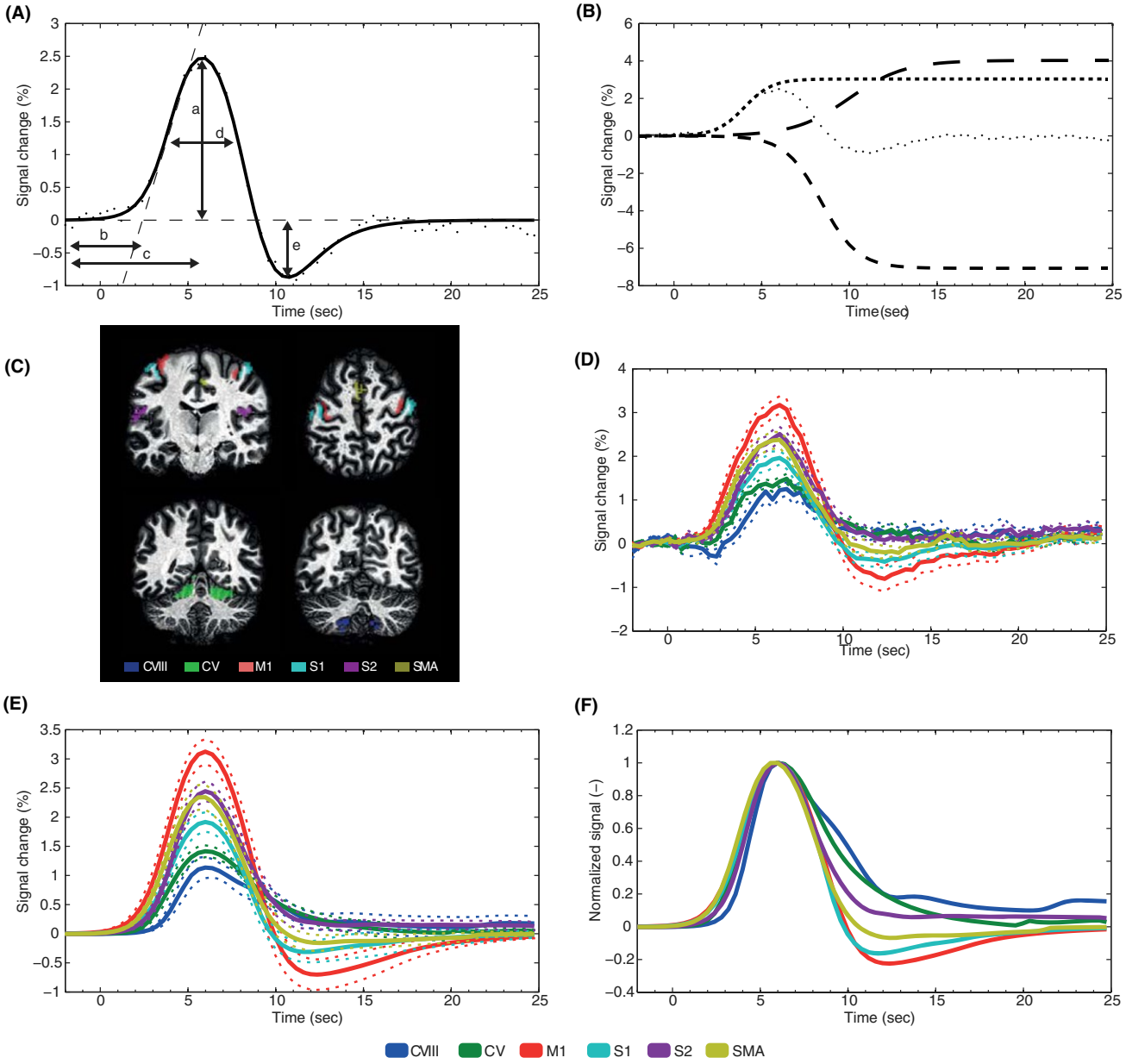

FIGURE 1 A, Example of a fitted positive BOLD response (PBR) and the measured parameters: positive peak height, measured as the maximum height from the baseline (A); time of onset, measured as the time of the intersection between the baseline and the fit of the first linear part of the positive peak (B); time to peak, measured as the time of the maximum height (C); FWHM of the positive peak (D); and the undershoot amplitude, measured as the maximal negative height from the baseline (E). B, Example of the 3 inverse logit function used to model the PBR. The first models the positive peak increase; the second models the decrease down to the undershoot; and the third models the return to baseline, as represented by the small, medium, and large dashed lines, respectively. C, The 6 bilateral regions of interest (ROIs) used to extract the PBRs: cerebellar lobule VIII (CVIII), cerebellar lobule V (CV), primary motor cortex (M1), primary somatosensory cortex (S1), secondary somatosensory cortex (S2), and supplementary motor area (SMA). D, Averaged raw time courses. E, Averaged fitted time courses (the dashed lines represent the SEM). F, Averaged fitted time courses normalized to the positive peak amplitude

and they may differ among brain regions. These differences may be especially prominent in regions with a different cellular and vascular organization, such as the cerebellum, where, to our knowledge, the PBR has never been characterized.

As the shape of the modeled BOLD response partially determines the success of general linear model analysis, spatial variations in PBR shape may influence the statistical significance of local BOLD responses. This is particularly relevant now that both higher SNR and BOLD contrast are available with higher B_0 and widely adopted new sequences[14-17] that allow very high temporal resolution. Using these sequences, full-brain data with an intermediate spatial resolution (approximately 2 mm) can be acquired in as little as 400-500 ms.[14,18,19] These subsecond acquisitions will

provide the greatest benefit in BOLD sensitivity when analyzed using an optimal PBR model. They can also be used to study the PBR shape. The purpose of this study was to precisely measure the temporal properties of the PBR response at 7 T in regions involved in motor control, including the cerebellum.

2 | METHODS

2.1 | Participants

Eight healthy participants (3 females; 19-24 years old; right handed) were scanned at 7 T (Siemens, Munich, Germany) using an insert gradient coil (AC84) and a 32-channel RF coil (Nova Medical, Wilmington, MA). All participants provided written informed consent, and the study was approved by the institutional review board of the local ethics committee (Commission d'Éthique de la Recherche sur l'Être Humain du Canton de Vaud). The guidelines of the Helsinki Declaration were followed throughout the study. Participants were asked not to consume any alcohol or caffeine during the 12 hours preceding the experiment.

2.2 | Paradigm

Two functional acquisitions were performed: first a "localizer" run during which the participants performed the finger-tapping task unilaterally (15 seconds ON, 30 seconds OFF, alternating for 9 minutes), whereby the cues for left-hand and right-hand movements were pseudo-randomly ordered. This was followed by an event-related run in which the participants were asked to make a single bimanual finger-tapping movement once every 30 seconds (for 7 minutes). For both tasks, finger tapping was performed as a fingers-to-thumb movement, in which the 4 fingers were simultaneously moved to touch the thumb. Participants rested their lower arms comfortably against the scanner bore during the entire run.

2.3 | Data acquisition

For the localizer, a 2D EPI sequence was used with $2 \times 2 \times 2$ mm voxels; 30 coronal-oblique slices with an in-plane FOV of 212×212 mm^2 were acquired per volume; and the following parameters were used: TR/TE/α = 2500 ms/26 ms/75º. An iPAT factor of 3 was used to reduce the readout length. Other parameters include bandwidth of 2246 Hz/pixel and slice gap of 1 mm. The imaging slab covered the cerebellum, primary and supplementary motor areas, and somatosensory cortices. Dielectric pads were used to improve signal homogeneity over the cerebellum.[20,21]

The event-related task was acquired with a fast 3D-EPI controlled aliasing in parallel imaging (CAIPI) protocol.[14] The 2D-CAIPIRINHA (controlled aliasing in parallel imaging results in higher acceleration) sampling scheme22 allows the acquisition of data with higher undersampling factors by improving the distribution of lines through k-space. A value of $\Delta_{CAIPIRINHA} = N$ indicates a shift of N planes in k-space per acquired line. Fast acquisitions with highly accelerated 3D-EPI-CAIPI are comparable to and sometimes outperform the more widely used simultaneous multislice EPI method.[23,24] Data were acquired with a nominal spatial resolution of $2 \times 2 \times 2$ mm in the same coronal–oblique orientation as the functional localizer data. The TR_{volume}/TR/TE/α were 399 ms/57 ms/27 ms/15º and FOV of $212 \times 176 \times 120$ mm^3. The bandwidth was 2774 Hz/pixel and the echo spacing 0.51 ms. For these acquisitions, an undersampling factor of 6 was used with $\Delta_{CAIPIRINHA}$ of 2 in combination with a partial Fourier factor $PF_z = 6/8$. No fat saturation was applied. For both functional runs, respiratory and cardiac traces were recorded with vendor-provided sensors. The physiological logs were marked with the scanner triggers to compensate for any differences in the clocks of the scanner and stimulus computer. An MP2RAGE data set was also acquired for an anatomical reference[25] using the following parameters: voxel size = $0.6 \times 0.6 \times 0.6$ mm^3, FOV = $192 \times 192 \times 154$ mm^3, TI1/TI2 = 800/2700 ms, and $TR_{MP2RAGE}$/TR/TE = 6000 ms/6.2 ms/3.03 ms.

2.4 | Data processing

The localizer data were slice-timing corrected, realigned, and analyzed with a general linear model (SPM12; https://www.fil.ion.ucl.ac.uk/spm/) to define 6 bilateral regions of interest (ROIs) (Figure 1C): primary motor cortex (M1), primary sensory cortex (S1), supplementary motor area (SMA), secondary sensory cortex (S2), cerebellum lobule V (CV), and cerebellum lobule VIII (CVIII). The M1 and S1 clusters were identified using the central sulci as a landmark. Additionally, as the M1 and S1 clusters were usually contiguous, these ROIs were manually delineated using MRIcron,[26] using the fundus of the central sulcus as the border. The SMA was identified as the significant cluster on the midline anterior to M1, and S2 was identified as a significant cluster of activity on the upper banks of the lateral sulci. The cerebellar clusters were found by locating clusters in lobule IV/V and VIII of the cerebellum. Each ROI contained between 100 and 400 voxels for a threshold of $P < .001$, uncorrected for multiple comparisons. At this stage, 1 participant was excluded from further analysis as no cerebellar ROIs were obtained. Three other volunteers only showed sufficient activity in the anterior lobe cluster in lobule V of the cerebellum.

The localizer data were coregistered to the motion-corrected 3D-EPI-CAIPI data. The time courses of the within-ROI voxels were then extracted from the CAIPI data using marsbar.[27] The time courses of all voxels were filtered and physiological signal fluctuations were removed using

regressors obtained from RETROICOR.[28] The time courses were then averaged across all voxels in the ROI, across the trials, and normalized to the baseline (2 seconds before stimulus onset).

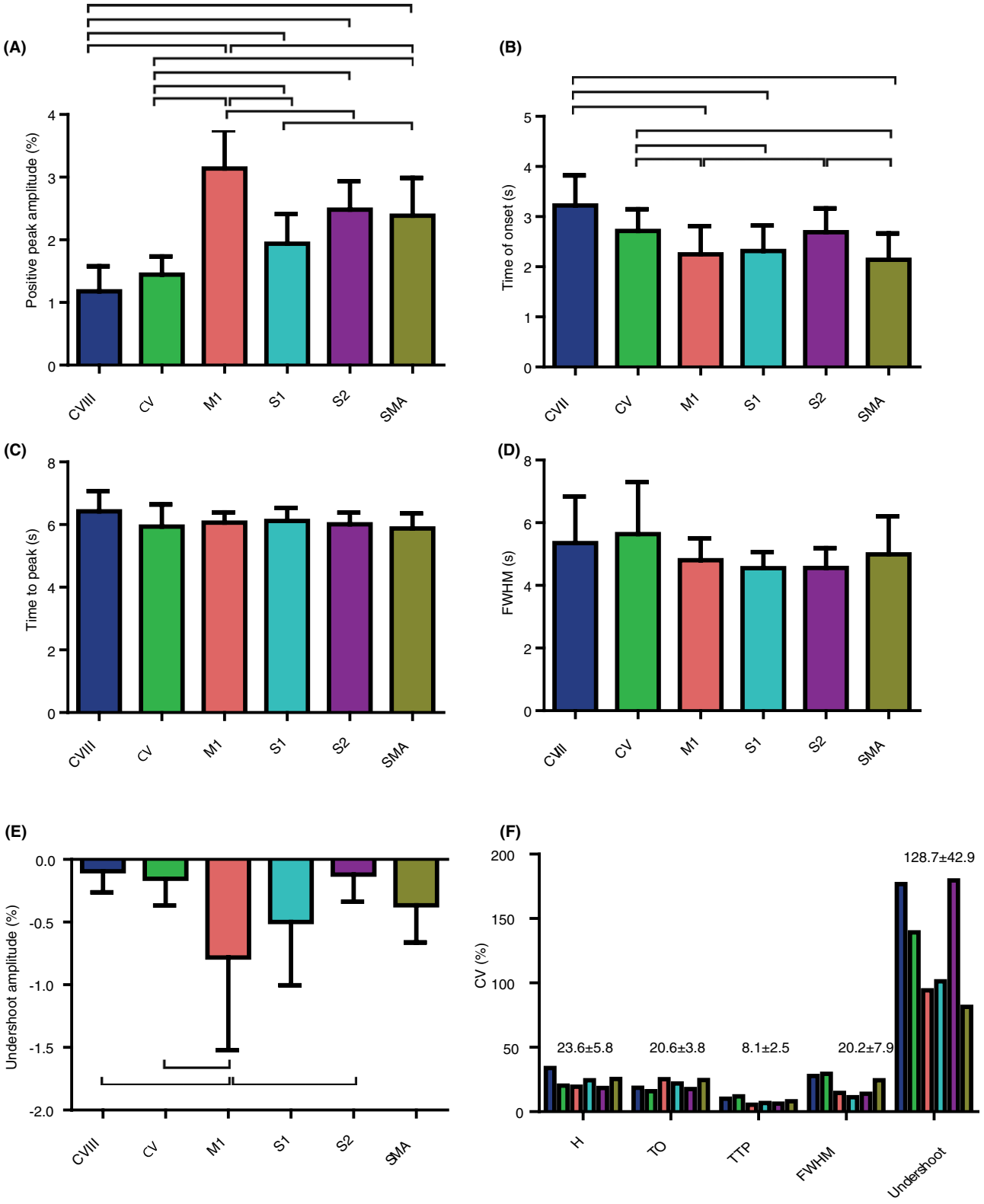

FIGURE 2 Measurements of the different PBR parameters for the 6 bilateral ROIs: positive peak amplitude (A), time of onset (B), time to peak (TTP) (C), FWHM (D), and undershoot amplitude (E). The bar plots represent the mean ± SD across participants. F, Intersubject coefficients of variation for each ROI and measurement computed as the SD divided by the mean. The values above the bar plots represent the mean ± SD across the 6 ROIs for each measurement

Three inverse logit functions[29,30] (Figure 1B) were fit to the averaged time courses using a restricted Nelder–Mead simplex algorithm. The positive peak height, time of onset, time to peak (TTP), FWHM, and the undershoot amplitude were extracted from the fitting results (Figure 1A). The positive peak and undershoot amplitudes were measured as the maximal and minimal values of the positive and subsequent negative peaks, respectively. To measure the time of onset, a linear fit was performed using the points between 20% and 80% of the positive peak height of the fitted response, with the time of onset corresponding to the time of intercept between the fit and the baseline level. The TTP corresponded to the time of the maximal value of the positive peak. The FWHM was measured as the time between the 2 points at half of the maximum of the positive peak. Repeated measures statistics using a linear mixed model with ROIs as repeated factors were performed independently, followed by post hoc analysis (significance level $P < .05$; familywise error).

3 | RESULTS

The acquisition slab position covered all ROIs, which together form the main cortical brain areas involved in motor function (Figure 1C), including cerebellar lobules V and VIII. No significant BOLD responses were found in the basal ganglia, so this region was not included in the analysis. The time courses averaged across participants from the 6 ROIs are shown in Figure 1D. Dotted lines indicate the SD across all subjects. The 30-second interstimulus interval was sufficiently long for this short motor stimulus to guarantee a return to baseline in all of the ROIs (Figure 1D). In addition to the difference in main height, the shape of the responses also clearly differs. Moreover, an initial dip can be seen in the CVIII time course, which, after looking at the single-subject time courses, was present only in half of the participants. The 3 inverse logit functions (Figure 1B) provided a good fit of the PBR time course (Figure 1E). The PBRs are also shown to be normalized for maximal peak height in Figure 1F to emphasize the differences in shape of the time courses.

Figure 2 depicts bar plots of the PBR measurements averaged over subjects. Error bars indicate the SD over subjects. The statistical analysis showed significant differences among the different ROIs, with main effects on the height of the peak ($F [5, 10.34] = 21.51$, $P < .001$; Figure 2A), the time of onset ($F [5, 13.08] = 6.81$, $P < .01$; Figure 2B), and the undershoot amplitude ($F [5, 32.36] = 5.30$, $P < .01$; Figure 2E). No significant differences were found for the TTP and FWHM (Figure 2C,D). Post hoc t tests showed that the peak height in M1 was greater than in any other region and that the cerebral regions showed on average higher amplitude compared with the cerebellar ROIs. The peak height difference between the S1 and M1 regions was notably larger.

In terms of timing, the PBR started later for the cerebellum, especially in CVIII, than in most of the cerebral ROIs. There was no significant difference in the onset times between the CVIII and CV ROIs.

Finally, the CV/CVIII ROIs and, to a smaller extent the S2 ROI, showed a significantly smaller undershoot amplitude compared with M1. Additionally, trends were also observed for the undershoot amplitude difference for the comparisons M1-S1 and M1-SMA. The difference in undershoot amplitudes was still present (Figure 1F) when the PBRs were normalized to the amplitude of the positive peak. For the intersubject variability of the 6 ROIs, the undershoot was the most variable measure, assessed by coefficient of variation (Figure 2F), whereas the TTP varied the least. Interestingly, no specific ROIs stood out in terms of between-subject variability for the 5 fitted parameters.

4 | DISCUSSION

The high BOLD sensitivity at 7 T and the high temporal resolution provided by a 3D-EPI-CAIPI acquisition were used to measure the hemodynamic response curve in 6 regions in the motor network, including the cerebellum. For each stimulus, a single finger tap was performed, which was sufficient to trigger a detectable hemodynamic response in the areas of interest. Between different regions involved in motor control, several significant differences in the amplitude and timing of the response were observed, namely, the positive peak amplitude, the time of onset, and the undershoot amplitude. M1 showed the highest amplitudes for both the positive peak and undershoot compared with other motor regions, whereas CV, CVIII, and S2 PBRs started later.

The amplitude of the positive peak has been shown to be correlated to stimulus intensity and neuronal activity,[31] and therefore might reflect the involvement of each region during the task. Additionally, the amplitude of the BOLD response has been linked to other parameters such as the resting-state fluctuation amplitude,[32] the baseline venous oxygenation state,[33] and the coupling between cerebral blood flow (CBF) and cerebral metabolic rate ($CMRO_2$).[34] For example, Vafaee and Gjedde[12] showed that the cerebellum had a different coupling between CBF and $CMRO_2$ than M1 and SMA during a finger-tapping task at different frequencies, which would affect the BOLD signal amplitudes.

The undershoot in cerebellar lobules V and VIII was consistently small, and even completely absent in half of the subjects, suggesting a region dependence of the PBR undershoot. The undershoot has been suggested to be a purely vascular phenomenon (i.e., to be caused either by delayed vascular compliance between CBF and cerebral blood volume[35,36] or by a faster return to baseline of CBF and cerebral blood volume compared with the calculated $CMRO_2$), which

could vary between regions.[37] However, these mechanisms are only valid in the long stimulation regime. Several studies have shown that short stimulations, like those used in this study, do not lead to observable changes in venous cerebral blood volume.[38-40] In this case, the undershoot amplitude is modulated by both the decrease in CBF and the time needed for $CMRO_2$ to return to baseline.[41] Alternatively, the post-stimulus undershoot can be caused, at least partially, by post-stimulus inhibitory neuronal modulation.[42-44] Interestingly, triggering both inhibitive GABAergic activity and excitatory glutamatergic activity in the cerebellum increases the local field potential and CBF to a greater extent than glutamatergic activity alone,[45,46] which, in case of a GABAergic origin of the undershoot in the forebrain, could explain the negligible undershoot in the cerebellum.

In the current study, the undershoot varied widely between both regions and subjects, whereas the positive peak height varied much less. This might be due to the lower SNR of the undershoot compared with the positive peak, which affects the estimation of the former, or the higher variability in the excitation-inhibition balance[34] during the undershoot period.

As no consistent initial dip was observed for most of the ROIs in our study, it was not included in the model. The relatively low number of repetitions in the event-related run did probably not yield sufficient SNR to observe this subtle feature of the BOLD response, if it was indeed present.[3] The event-related motor responses were visually cued and may not have been sufficiently synchronized to resolve the dip. Only the CVIII PBR showed an initial dip, which was only present in half of the participants. A pronounced initial dip might lead to a delayed onset of the positive peak, as more time is needed for the BOLD signal to recover from below the baseline, and could potentially explain the late onset of the CVIII PBR.

No significant differences were observed in the TTP here. Previous studies showed that the TTP of the positive peak varies little among most of the significant regions during unimodal[47] or multimodal[48] stimulations. In our case, we found only significant differences for the TO, with the cerebellar PBR and S2 PBR starting to increase later than the other brain regions. This is partially consistent with previous results, indicating that the peaks of higher amplitude due to different stimulus intensities start earlier when using a long interstimulus interval,[49] as was the case in the current study, although, in our data, S1, S2, and SMA do not appear to follow this observation. Therefore, differences in time of onset may be related to the number of neurons stimulated in each region during the task, to the timing of their activation, or the latencies of the CBF and $CMRO_2$ responses.

In this study, the response observed is referred to as the PBR. The term "hemodynamic response function" is also often used in fMRI studies to characterize BOLD responses. However, as we investigated the variability of functional responses across different brain regions, the underlying neuronal activity is likely to differ, so we chose to use the more generic term of PBR.

Using high temporal resolution to sample the BOLD signal, our study provided precise measurements of the PBR across the motor regions, including the cerebellum, a structure that is difficult to visualize adequately using MRI. Despite several hypothesis that may explain the observed differences of timings and amplitudes, further studies are required to determine whether the observed changes are purely of vascular or neuronal origin. Additionally, because of its unique and well-characterized cellular organization, the cerebellum represents an interesting structure to investigate neurovascular coupling.

ACKNOWLEDGMENTS

We thank Dr. Hikari Yoshihara for commenting and proofreading the manuscript. This work was supported by the Centre d'Imagerie BioMédicale of the Universités de Lausanne, Université de Genéve, Hôpitaux Universitaires Genéve, Centre Hospitalier Universitaire Vaudois, and Ecole Polytechnique Fédérale de Lausanne; the Leenaards and Jeantet Foundations; and the Swiss National Science Foundation (31003A_149983 and 31003A_153070).

REFERENCES

1. Ogawa S, Lee T-M. Magnetic resonance imaging of blood vessels at high fields: in vivo and in vitro measurements and image simulation. *Magn Reson Med*. 1990;16:9–18.
2. Bandettini PA, Wong EC, Hinks RS, Tikofsky RS, Hyde JS. Time course EPI of human brain function during task activation. *Magn Reson Med*. 1992;25:390–397.
3. Hu X, Yacoub E. The story of the initial dip in fMRI. *NeuroImage*. 2012;62:1103–1108.
4. Uludağ K. To dip or not to dip: reconciling optical imaging and fMRI data. *PNAS*. 2010;107:E23, author reply E24.
5. Handwerker DA, Ollinger JM, D'Esposito M. Variation of BOLD hemodynamic responses across subjects and brain regions and their effects on statistical analyses. *NeuroImage*. 2004;21:1639–1651.
6. Aguirre GK, Zarahn E, D'esposito M. The variability of human, BOLD hemodynamic responses. *NeuroImage*. 1998;8:360–369.
7. Laurienti PJ, Field AS, Burdette JH, Maldjian JA, Yen YF, Moody DM. Dietary caffeine consumption modulates fMRI measures. *NeuroImage*. 2002;17:751–757.
8. Henson R, Price CJ, Rugg MD, Turner R, Friston KJ. Detecting latency differences in event-related BOLD responses: application to words versus nonwords and initial versus repeated face presentations. *NeuroImage*. 2002;15:83–97.

9. D'Esposito M, Zarahn E, Aguirre GK, Rypma B. The effect of normal aging on the coupling of neural activity to the bold hemodynamic response. *NeuroImage*. 1999;10:6–14.
10. D'Esposito M, Deouell LY, Gazzaley A. Alterations in the BOLD fMRI signal with ageing and disease: a challenge for neuroimaging. *Nat Rev Neurosci*. 2003;4:863–872.
11. Lecrux C, Hamel E. Neuronal networks and mediators of cortical neurovascular coupling responses in normal and altered brain states. *Philos Trans R Soc B Biol Sci*. 2016;371:20150350.
12. Vafaee MS, Gjedde A. Spatially dissociated flow-metabolism coupling in brain activation. *NeuroImage*. 2004;21:507–515.
13. Rossini PM, Altamura C, Ferretti A, et al. Does cerebrovascular disease affect the coupling between neuronal activity and local haemodynamics? *Brain*. 2004;127:99–110.
14. Narsude M, Gallichan D, Van Der Zwaag W, Gruetter R, Marques JP. Three-dimensional echo planar imaging with controlled aliasing: a sequence for high temporal resolution functional MRI. *Magn Reson Med*. 2016;75:2350–2361.
15. Barth M, Breuer F, Koopmans PJ, Norris DG, Poser BA. Simultaneous multislice (SMS) imaging techniques. *Magn Reson Med*. 2016;75:63–81.
16. Poser BA, Setsompop K. Pulse sequences and parallel imaging for high spatiotemporal resolution MRI at ultra-high field. *NeuroImage*. 2016;1–18.
17. Setsompop K, Gagoski BA, Polimeni JR, Witzel T, Wedeen VJ, Wald LL. Blipped-controlled aliasing in parallel imaging for simultaneous multislice echo planar imaging with reduced g-factor penalty. *Magn Reson Med*. 2012;67:1210–1224.
18. Feinberg DA, Moeller S, Smith SM, et al. Multiplexed echo planar imaging for sub-second whole brain fMRIand fast diffusion imaging. *PLoS One*. 2010;5.
19. Uğurbil K, Xu J, Auerbach EJ, et al. Pushing spatial and temporal resolution for functional and diffusion MRI in the Human Connectome Project. *NeuroImage*. 2013;80:80–104.
20. Teeuwisse WM, Brink WM, Webb AG. Quantitative assessment of the effects of high-permittivity pads in 7 Tesla MRI of the brain. *Magn Reson Med*. 2012;67:1285–1293.
21. Vaidya MV, Lazar M, Deniz CM, et al. Improved detection of fMRI activation in the cerebellum at 7T with dielectric pads extending the imaging region of a commercial head coil. *J Magn Reson Imaging*. 2018;1–10.
22. Breuer FA, Blaimer M, Mueller MF, et al. Controlled aliasing in volumetric parallel imaging (2D CAIPIRINHA). *Magn Reson Med*. 2006;55:549–556.
23. Reynaud O, Jorge J, Gruetter R, Marques JP, van der Zwaag W. Influence of physiological noise on accelerated 2D and 3D resting state functional MRI data at 7 T. *Magn Reson Med*. 2017;78:888–896.
24. Stirnberg R, Huijbers W, Brenner D, Poser BA, Breteler M, Stöcker T. Rapid whole-brain resting-state fMRI at 3 T: efficiency-optimized three-dimensional EPI versus repetition time-matched simultaneous-multi-slice EPI. *NeuroImage*. 2017;163:81–92.
25. Marques JP, Kober T, Krueger G, van der Zwaag W, Van de Moortele P-F, Gruetter R. MP2RAGE, a self bias-field corrected sequence for improved segmentation and T1-mapping at high field. *NeuroImage*. 2010;49:1271–1281.
26. Rorden C, Brett M. Stereotaxic display of brain lesions. *Behav Neurol*. 2000;12:191–200.
27. Brett M, Anton JL, Valabregue R, Poline JB. Region of interest analysis using an SPM toolbox. In: Proceedings of the 8th International Conference on Functional Mapping of the Human Brain, Sendai, Japan; 2002: 10511.
28. Glover GH, Li TQ, Ress D. Image-based method for retrospective correction of physiological motion effects in fMRI: RETROICOR. *Magn Reson Med*. 2000;44:162–167.
29. Lindquist MA, Meng Loh J, Atlas LY, Wager TD. Modeling the hemodynamic response function in fMRI: efficiency, bias and mis-modeling. *NeuroImage*. 2009;45:S187–S198.
30. Lindquist MA, Wager TD. Validity and power in hemodynamic response modeling: a comparison study and a new approach. *Hum Brain Mapp*. 2007;28:764–784.
31. Logothetis NK, Pauls J, Augath M, Trinath T, Oeltermann A. Neurophysiological investigation of the basis of the fMRI signal. *Nature*. 2001;412:150–157.
32. Kannurpatti SS, Rypma B, Biswal BB. Prediction of task-related BOLD fMRI with amplitude signatures of resting-state fMRI. *Front Syst Neurosci*. 2012;6:1–10.
33. Lu H, Yezhuvath US, Xiao G. Improving fMRI sensitivity by normalization of basal physiologic state. *Hum Brain Mapp*. 2010;31:80–87.
34. Buxton RB, Griffeth V, Simon AB, Moradi F. Variability of the coupling of blood flow and oxygen metabolism responses in the brain: a problem for interpreting BOLD studies but potentially a new window on the underlying neural activity. *Front Neurosci*. 2014;2:1–6.
35. van Zijl P, Hua J, Lu H. The BOLD post-stimulus undershoot, one of the most debated issues in fMRI. *NeuroImage*. 2012;62:1092–1102.
36. Buxton RB, Wong EC, Frank LR. Dynamics of blood flow and oxygenation changes during brain activation: the ballon model. *Magn Reson Med*. 1998;39:855–864.
37. Donahue MJ, Blicher JU, Østergaard L, et al. Cerebral blood flow, blood volume, and oxygen metabolism dynamics in human visual and motor cortex as measured by whole-brain multimodal magnetic resonance imaging. *J Cereb Blood Flow Metab*. 2009;29:1856–1866.
38. Drew PJ, Shih AY, Kleinfeld D. Fluctuating and sensory-induced vasodynamics in rodent cortex extend arteriole capacity. *Proc Natl Acad Sci*. 2011;108:8473–8478.
39. Hillman E, Devor A, Bouchard MB, et al. Depth-resolved optical imaging and microscopy of vascular compartment dynamics during somatosensory stimulation. *NeuroImage*. 2007;35:89–104.
40. Vazquez AL, Fukuda M, Tasker ML, Masamoto K, Kim SG. Changes in cerebral arterial, tissue and venous oxygenation with evoked neural stimulation: implications for hemoglobin-based functional neuroimaging. *J Cereb Blood Flow Metab*. 2010;30:428–439.
41. Kim JH, Ress D. Arterial impulse model for the BOLD response to brief neural activation. *NeuroImage*. 2016;124:394–408.
42. Mullinger KJ, Mayhew SD, Bagshaw AP, Bowtell R, Francis ST. Poststimulus undershoots in cerebral blood flow and BOLD fMRI responses are modulated by poststimulus neuronal activity. *Proc Natl Acad Sci U S A*. 2013;110:13636–13641.
43. Mullinger KJ, Cherukara MT, Buxton RB, Francis ST, Mayhew SD. Post-stimulus fMRI and EEG responses: evidence for a neuronal origin hypothesised to be inhibitory. *NeuroImage*. 2017;157:388–399.

44. Sadaghiani S, Uğurbil K, Uludağ K. Neural activity-induced modulation of BOLD poststimulus undershoot independent of the positive signal. *Magn Reson Imaging*. 2009;27:1030–1038.
45. Caesar K, Gold L, Lauritzen M. Context sensitivity of activity-dependent increases in cerebral blood flow. *Proc Natl Acad Sci U S A*. 2003;100:4239–4244.
46. Lauritzen M, Mathiesen C, Schaefer K, Thomsen KJ. Neuronal inhibition and excitation, and the dichotomic control of brain hemodynamic and oxygen responses. *NeuroImage*. 2012;62:1040–1050.
47. Jorge J, Figueiredo P, Gruetter R, van der Zwaag W. Mapping and characterization of positive and negative BOLD responses to visual stimulation in multiple brain regions at 7T. *Hum Brain Mapp*. 2018;39:2426–2441.
48. Taylor AJ, Kim JH, Ress D. Characterization of the hemodynamic response function across the majority of human cerebral cortex. *NeuroImage*. 2018;173:322–331.
49. Thompson SK, Engel SA, Olman CA. Larger neural responses produce BOLD signals that begin earlier in time. *Front Neurosci*. 2014;8:159.

How to cite this article: Boillat Y, van der Zwaag W. Whole brain measurements of the positive BOLD response variability during a finger tapping task at 7 T show regional differences in its profiles. *Magn Reson Med*. 2019;81:2720–2727. https://doi.org/10.1002/mrm.27566